Evaporated lithium surface coatings in NSTX

H.W. Kugel [a,*], D. Mansfield [a], R. Maingi [b], M.G. Bell [a], R.E. Bell [a], J.P. Allain [c], D. Gates [a], S. Gerhardt [a], R. Kaita [a], J. Kallman [a], S. Kaye [a], B. LeBlanc [a], R. Majeski [a], J. Menard [a], D. Mueller [a], M. Ono [a], S. Paul [a], R. Raman [d], A.L. Roquemore [a], P.W. Ross [a], S. Sabbagh [e], H. Schneider [a], C.H. Skinner [a], V. Soukhanovskii [f], T. Stevenson [a], J. Timberlake [a], W.R. Wampler [g], J. Wilgren [b], L. Zakharov [a], The NSTX Team

[a] Princeton Plasma Physics Laboratory, Princeton, P.O. Box 451, NJ 08543, USA
[b] Oak Ridge National Laboratory, Oak Ridge, TN 37831, USA
[c] Purdue University, School of Nuclear Engineering, West Lafayette, IN 47907, USA
[d] University of Washington, Seattle, WA 98195, USA
[e] Columbia University, New York, NY 10027, USA
[f] Lawrence Livermore National Laboratory, Livermore, CA 94551, USA
[g] Sandia National Laboratories, Albuquerque, NM 87185, USA

ARTICLE INFO

ABSTRACT

Two lithium evaporators were used to evaporate more than 100 g of lithium on to the NSTX lower divertor region. Prior to each discharge, the evaporators were withdrawn behind shutters, where they also remained during the subsequent HeGDC applied for periods up to 9.5 min. After the HeGDC, the shutters were opened and the LITERs were reinserted to deposit lithium on the lower divertor target for 10 min, at rates of 10–70 mg/min, prior to the next discharge. The major improvements in plasma performance from these lithium depositions include: (1) plasma density reduction as a result of lithium deposition; (2) suppression of ELMs; (3) improvement of energy confinement in a low-triangularity shape; (4) improvement in plasma performance for standard, high-triangularity discharges; (5) reduction of the required HeGDC time between discharges; (6) increased pedestal electron and ion temperature; (7) reduced SOL plasma density; and (8) reduced edge neutral density.

© 2009 Elsevier B.V. All rights reserved.

1. Introduction

The National Spherical Torus Experiment (NSTX) [1,2] has been investigating lithium (Li) coatings for density and impurity control [3,4]. In NSTX, recycling of hydrogenic species from the plasma contact with graphite surfaces, contributes to a secular density rise observed in most H-mode, neutral beam injection (NBI) heated plasmas [5]. Plasma efflux incident on elemental Li can form LiD, thereby making it unavailable for recycling. However, Li reactions with gas embedded in the graphite (e.g. resulting in LiD, LiOH, LiOD, Li_2CO_3) are believed to make it unavailable to combine with incident deuterium ions and neutrals to form LiD, and thereby unable to provide density pumping. Earlier NSTX Li Pellet Injection experiments [3] with degassed limiters and divertors obtained results similar to the experience with Li coatings in TFTR [6], and with a liquid-lithium limiter in the Current Drive Experiment-Upgrade (CDX-U) [7]. More recent NSTX work has been with thermally evaporated Li coatings for performing routine Li coating over a significant fraction of the graphite plasma facing surfaces [4].

Benefits from the Li coatings were sometimes, but not always seen [4]. These benefits sometimes included decreases in plasma density, inductive flux consumption, and edge-localized mode (ELM) occurrence, and increases in electron temperature, ion temperature, energy confinement, and periods of edge and magnetohydrodynamic (MHD) quiescence [4]. In addition, reductions in lower divertor D, C, and O luminosity were measured. These results motivated the installation of a second additional Li evaporator for performing routine solid Li coatings, at high rates, between plasma discharges, over the entire lower divertor surface. This work describes initial results from these experiments using two Li evaporators.

2. Experiment description

Typical NSTX parameters are $R_0 \leqslant 0.85$ m, $a \leqslant 0.67$ m, $R/a \geqslant 1.26$, $\kappa \leqslant 2.7$, $\delta \leqslant 0.8$, $I_p \leqslant 1.5$ MA, $B_T \leqslant 0.55$ T, and 1.5 s maximum pulse length [1,2]. Copper passive stabilizer plates, graphite power handling surfaces, 7 MW of deuterium Neutral Beam Injection (NBI) heating, and 6 MW of 30 MHz High Harmonic Fast Wave (HHFW) power for radio frequency (rf) heating and current drive provide additional experimental versatility. The 0.2 m radius

center stack (CS) is clad with alternating vertical columns of 1.3 cm thick graphite (Union Carbide, Type ATJ) tiles between columns of 2-D Carbon Fiber Composite (Allied Signal, Type 865-19-4) tiles. The inner divertor tiles are 5.1 cm thick Type ATJ graphite; the outer divertor and passive stabilizer plate tiles are 2.5 cm thick Type ATJ graphite. The PFCs are conditioned as required using vacuum bakeout at 350 °C, Helium Glow Discharge C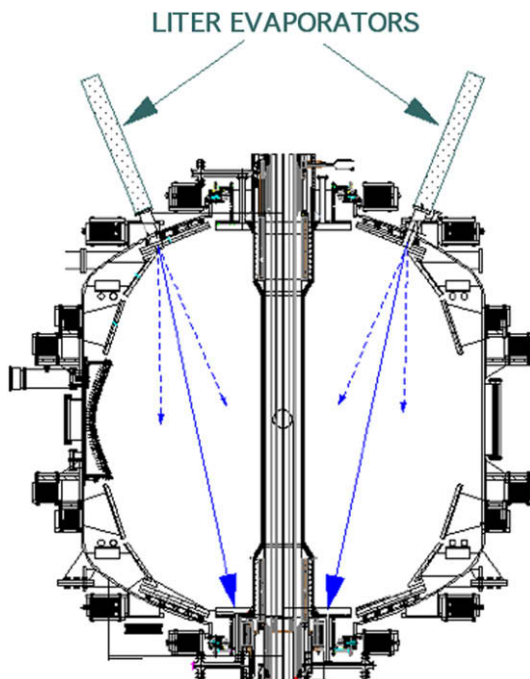leaning (HeGDC) between discharges and boronization [8]. Fig. 1 shows a schematic diagram of the poloidal cross section of NSTX, the locations of two LIThium EvaporatoRs (LITERs) at toroidal angles 165° and 315°, the LITER central-axis aimed at the lower divertor, and dashed lines indicating the gaussian half-angles at $1/e$ intensity of the measured evaporated Li angular distributions. Four in-vessel Quartz Deposition Monitors (QDM) were used as independent monitors of the Li deposition rate [9] between discharges compared to the deposition rate as inferred from the LITER oven temperature [4]. Typical evaporation rates have been in the range 10–70 mg/min (5–40 mg/min per LITER unit). The measured LITER oven temperatures were used together with the laboratory calibration measurements to determine the total evaporated Li between discharges [4]. Due to the thermal inertia of the LITER units, they are operated continuously during the experimental day at a selected rate. However, at about −60 s before each discharge, the LITER units are retracted from their operating positions to locations behind Li-blocking shutters. After the discharge, if a HeGDC is performed, the Li shutters remain closed until the HeGDC is completed. This is done so as to prevent codepositon of Li and He, and the subsequent outgassing of He during the following deuterium discharge. After the shutters are opened, the LITER units are inserted to their operating positions, and a 10 min evaporation deposits Li onto the lower divertor target. During the work reported here, Li depositions from a 200 to 700 mg were applied between discharges. The total Li applied was more than 100 g. This Li amount would correspond to a thickness of at least 2.4×10^{-2} cm if averaged over the NSTX lower divertor, or 4.7×10^{-4} cm if averaged over the interior of NSTX.

In this work, several lower single null diverted (LSND) deuterium reference discharges were taken prior to the deposition of Li. These consisted of a LSND low-triangularity discharge (B_t = 0.5 T, I_p = 800 kA, δ = 0.5, κ = 1.8, 3 NBI) and a LSND high-triangularity discharge (B_t = 0.5 T, I_p = 900 kA, δ = 0.8, κ = 2.3, 3 NBI). Following the deposition of Li at various rates and amounts, the resultant edge conditions were tested using the same LSND deuterium reference discharge. During this work, it was attempted to keep the gas fueling, NB power and timing, and other operating conditions constant so as measure the effects of Li coatings under constant discharge conditions. However, as the operating day progressed, and the deposited Li amount preceding each discharge increased, it was found necessary to make operating changes. To keep the density from falling too low, and either the discharge being terminated early, or in a locked mode, more fueling was required. Input power was limited to avoid a beta limit as stored energy increased and flux consumption decreased. Maintaining approximately the same density (when required for a particular experiment) was done by varying the gas sources and their timing, and varying the NB timing.

3. Experimental results

Fig. 2 shows a comparison for pre-Li and post-Li (8537 mg) reference shots with constant NBI, external gas, and operating parameters showing how Li edge conditions reduce ELMs, and increase confinement, stored energy, and pulse length. Fig. 3 shows a database of total plasma electrons versus total electrons of the injected deuterium gas fuel, showing Li edge conditions require large fueling increases to maintain density and constant discharge condi-

Fig. 1. Schematic diagram of the poloidal cross section of NSTX, the locations of the two LIThium EvaporatoRs (LITERs) at toroidal angles 165° and 315°, and the LITER central-axis aimed at the lower divertor, and dashed lines indicating the gaussian half-angles at $1/e$ intensity of the measured evaporated Li angular distributions.

Fig. 2. Comparison for pre-Li and post-Li reference shots with constant NBI, constant external gas, and operating parameters showing how Li edge conditions reduce ELMs (F), and increase confinement (E), stored energy (D), and pulse length (A).
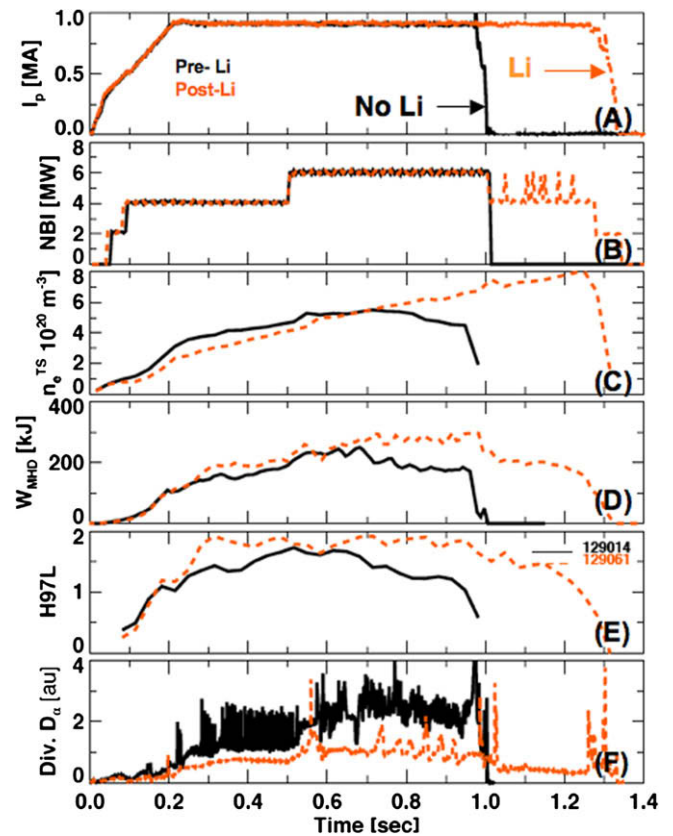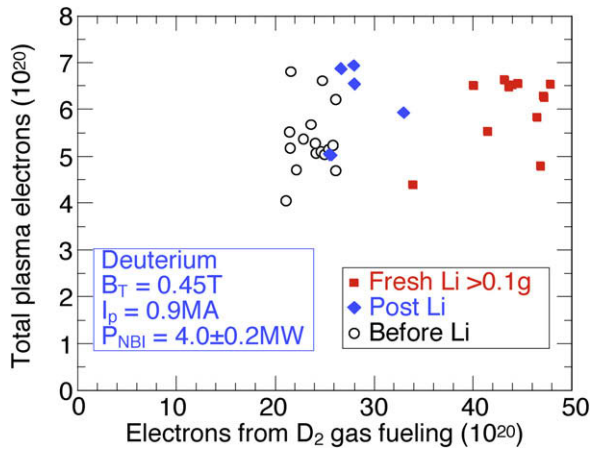
Fig. 3. A database of total plasma electrons *versus* total electrons of the injected deuterium gas fuel showing Li edge conditions require large fueling increases to maintain density and constant discharge conditions.
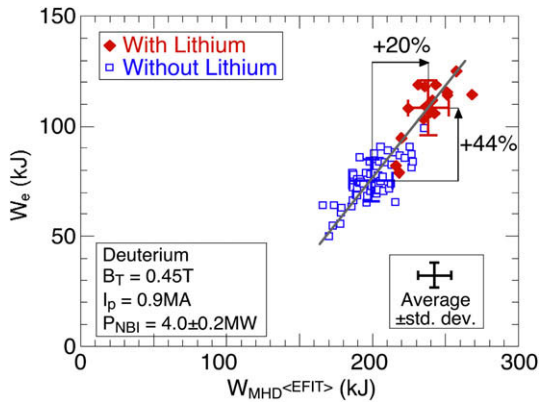

Fig. 4. A database of electron stored energy (W_e) *versus* total stored energy (W_{MHD}) for deuterium reference plasmas immediately following Li deposition, and for deuterium reference plasmas prior to Li deposition showing stored energy increases after Li deposition mostly through increase in electron stored energy. The EFIT equilibrium analysis is constrained by external magnetics, electron profile shape, and diamagnetic flux.

tions. Fig. 4 shows a database of electron stored energy (W_e) *versus* total stored energy (W_{MHD}) for deuterium reference plasmas immediately following Li deposition, and for deuterium reference plasmas prior to Li deposition, showing stored energy increases after Li deposition mostly through increase in electron stored energy. Fig. 5(A) shows a database of central electron temperature ($T_e(0)$) *versus* average electron temperature ($\langle T_e \rangle$) at the time of peak $\langle T_e \rangle$, with and without Li edge conditions, and Fig. 5(B) shows for the same discharges at the time of peak $\langle T_e \rangle$, the integrated loop voltage (Wb) *versus* the integrated torodial current (MC). It appears that the improvement in confinement with Li is mainly through broadening of the electron temperature profile. The broader electron temperature profile reduces the internal inductance (l_i) and inductive flux consumption, but as the discharge progresses impurity confinement increases, and higher Z_{eff} increases resistive flux consumption in the current (I_p) flattop. Fig. 6 gives a comparison for pre-Li and post-Li reference shots, showing Li edge conditions mitigate ELMs, increase stored energy, and lengthen pulse. Typically in recent NSTX experiments, He Glow Discharge Cleaning (HeGDC) has been required between discharges for 6–10 min to maintain the reproducibility of the subsequent H-mode discharges (i.e., the same H-mode transition time, H-mode power threshold, and pulse length). Fig. 7 shows the effects on H-mode pulse length
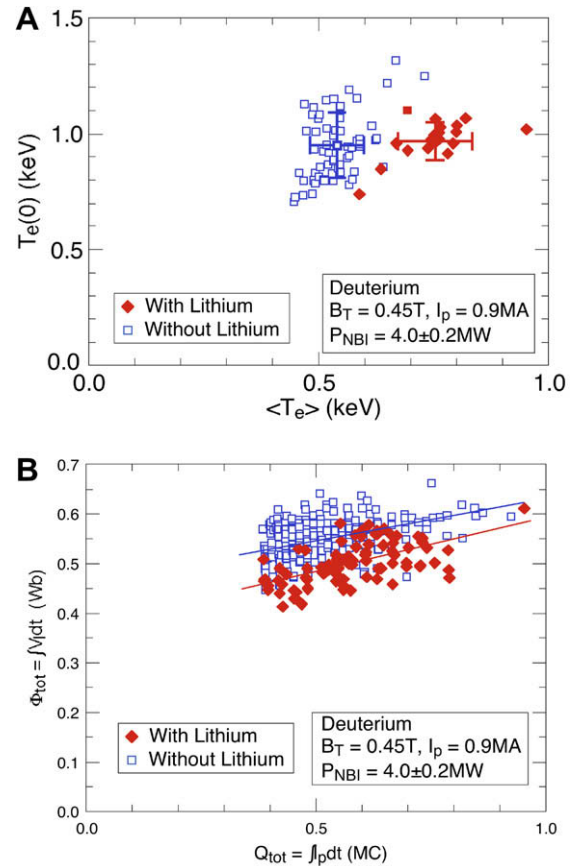

Fig. 5. (A) A database of central electron temperature ($T_e(0)$) *versus* average electron temperature ($\langle T_e \rangle$) at the time of peak $\langle T_e \rangle$, with and without Li edge conditions, and (B), shows for the same discharges at the time of peak $\langle T_e \rangle$, the integrated loop voltage (Wb) *versus* the integrated torodial current (MC). In (B) the solid lines are a guide to the eye.
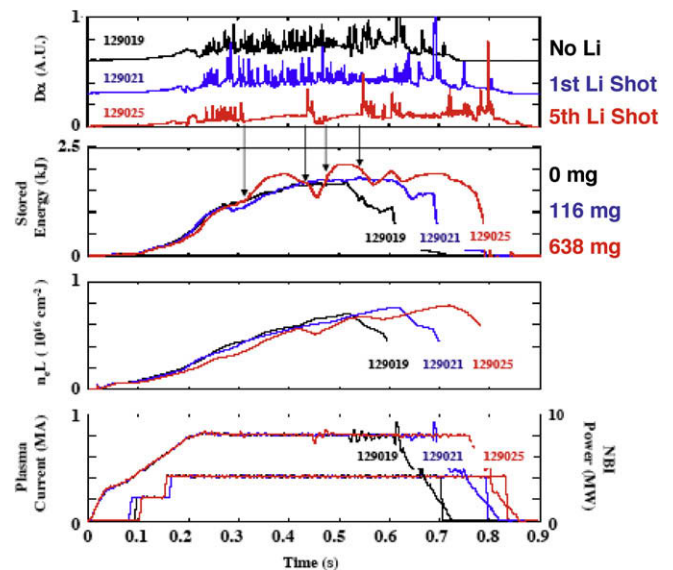

Fig. 6. Comparison for pre-Li and post-Li reference shots showing Li edge conditions mitigate ELMs, increase stored energy, and lengthen pulse.

of varying amounts of applied HeGDC duration and Li deposition. Reference shots were taken following 9.5 min of HeGDC and with no Li deposition between shots (Fig. 7(A)). Then the HeGDC was
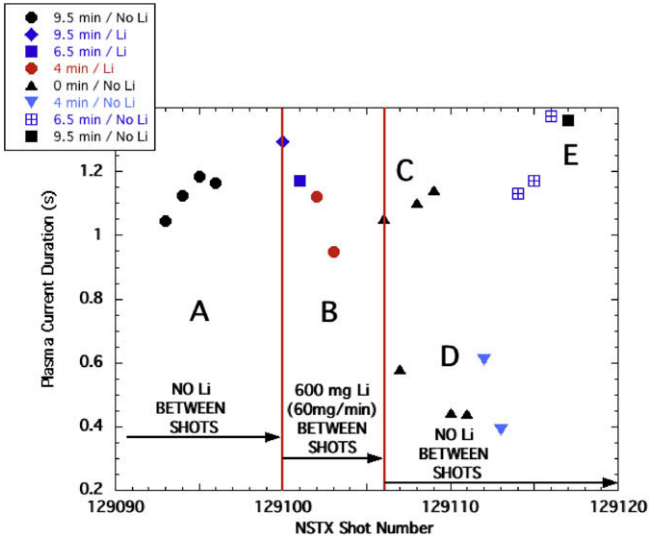
Fig. 7. Shown are the effects on H-mode pulse length of varying amounts of applied HeGDC duration and Li deposition. (A) Reference shots were taken following 9.5 min of HeGDC and no Li between shots. (B) The HeGDC shortened from 9.5 to 4 min followed by 10 min Li deposition. (C) No HeGDC and no Li deposition were performed between discharges. Initially there was no change at (C) no change, but by (D) conditions degrade. Reapplication of HeGDC (E) restored and exceeded initial conditions (A).

shortened from 9.5 to 4 min and followed by 10 min Li deposition (Fig. 7(B)). Following this, no HeGDC and no Li deposition was performed between discharges (Fig. 7(C)). Initially there was no change (Fig. 7(C)), but eventually conditions degraded (Fig. 7(D)). Reapplication of HeGDC (Fig. 7(E)) restored and exceeded initial conditions (Fig. 7(A)). These results demonstrate that Li edge conditions allowed H-mode plasma pulse lengths to be maintained with reduced or no HeGDC. Fig. 8 shows results following Li edge conditions after a Li deposition rate of 70 mg/min for 10 min, with a total of 5734 mg deposited in the vessel. Z-effective measurements for carbon from charge exchange spectroscopy, and Z-effective measurements for metals from bolometry measurements (Fig. 8(D)) [10] for this discharge show increasing impurity concentration. Fig. 8(C) shows how initially the core deuterium density to total electron density ratio is ~1 early in the discharge, but then decreases with increasing discharge pulse time, and simultaneously this dilution of core deuterium density reduces the measured D–D neutron production rate (Fig. 8(B)). The continuing rise in total density (N_e) in this discharge is discussed below.

4. Discussion

The behavior of ions and neutrals incident on solid Li to form LiD provides a pumping effect studied in this work [11]. In previous NSTX work, solid Li coatings were evaporated on the lower divertor
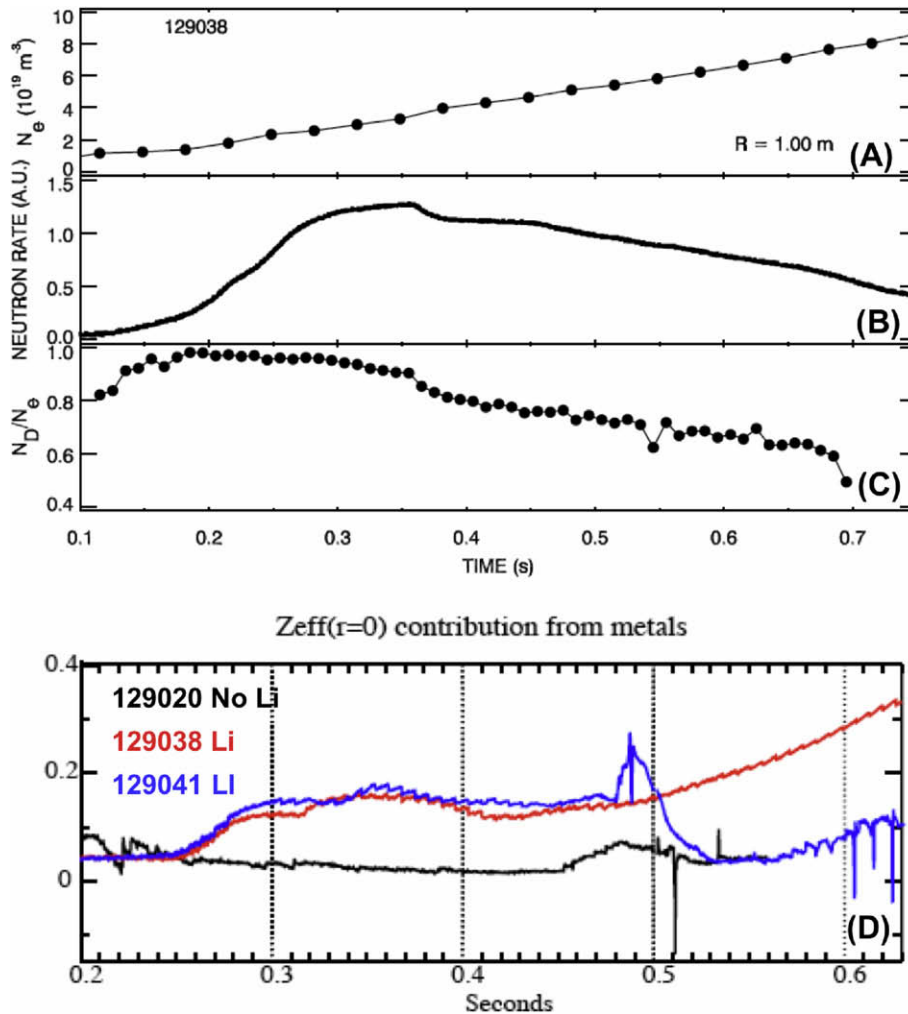

Fig. 8. (A) central density, (B) neutron rate, and (C) ratio of core deuterium density (N_D) to central electron density, and (D) Z-effective show that during Li edge conditions, as core deuterium-to-central density ratio decreases and neutron rate decreases.

target using one LITER unit. The thermal inertia of LITER is high, and this prevented the rapid cessation of evaporation prior to the application of HeGDC and the subsequent discharge. Hence, Li was evaporated directly into HeGDC. Although this 'lithiumization', which is similar to the well-known process of boronization, resulted in the deposition of Li on nearby PFCs, it also decreased the amount of Li that would be deposited directly on the divertor in the absence of HeGDC. In addition, direct evaporation into the HeGDC resulted in the codeposition of He in the Li coatings during the HeGDC. This effect, due to He trapping in solid Li [12], resulted in the slow outgassing of He on a time scale sufficient to dilute and perturb the subsequent deuterium discharge. In addition, Li was evaporated directly into discharges that resulted in undesirable coatings on diagnostic viewports in the line-of-sight from LITER. The work reported in this paper used 2 LITER units with newly-installed Li shutters that allow more flexible Li wall conditioning. The LITER shutters closed before the diagnostic window shutters opened, thereby avoiding window coating during the discharge. The closed Li shutters also allowed the HeGDC process to be applied without codeposition of He in the Li coatings, thereby avoiding He dilution of deuterium discharges.

The amount of incident deuterium ions and neutrals that can be pumped by a solid Li coating on the plasma wetted area is determined by the depth range of the incident particles. At typical NSTX plasma energies, the range of deuterium is about 100–250 nm. [13] As the central Li thickness directly under LITER increases, the coating of regions far from LITER grows in sufficient thickness to stop incident particles and form LiD. Hence, the effective pumping area is extended. Nuclear reaction analysis of graphite tiles after venting following experiments with one LITER unit, found that the deposited Li did not diffuse into the graphite beyond a few micrometer [14]. The use of 2 LITER units provided more uniform and rapid coverage of the lower divertor graphite surfaces. The shuttered operation avoided codeposition of Li with He. These improvements resulted in the relatively prompt response of noteworthy changes in plasma performance to small and rapid depositions of Li.

In comparisons of pre-Li and post-Li reference shots with constant external gas, constant NBI, and constant operating conditions (Fig. 2), a difference in early density with Li can clearly be seen. This was despite the fact that the reference discharge was ELMy (i.e., periodically purging density) and the Li shot was not. In time, the lack of ELMs begins to affect the density of the Li discharge, i.e., the rate of rise of electron density, and its density increases, and the pulse length continues beyond that of the pre-Li reference discharge. The effect on ELM mitigation is a noteworthy feature of Li edge conditions. Work is in progress to understand how Li edge conditions modify the SOL and pedestal properties and the relation of these changes to ELM behavior. Recent results on ELM mitigation are discussed elsewhere in this Conference [15].

The fueling changes up to $\times 2$ were needed (Fig. 3) to keep the plasma density from falling too low, and the plasma either being terminated early by a locked mode, or later by a beta limit as stored energy increased and flux consumption decreased, are indicative of the Li pumping effects. This suggests that future experiments with more extensive solid and liquid Li PFC coatings may require fueling beyond present capacities. Fig. 8 shows how initially the core deuterium density to total electron density ratio is ~ 1 in the discharge, but then decreases with increasing discharge pulse time, and the measured D–D neutron production rate decreases. The density (N_e) is seen to be increasing slowly early in the discharge and then increases at a faster rate after the core deuterium to total electron density starts decreasing. The continuing

rise in central density (N_e) in this discharge (Fig. 8(A)) appears to be due in part to the continued gas fueling needed to keep the plasma density from falling too low, and to an increasing Z_{eff} due to confined lithium, carbon, and metal impurities. Future work is needed to determine the respective contributions of fueling, residual recycling, and the amounts and origins of the confined impurities.

In conclusion, in recent experiments, the dual LITER system evaporated more than 100 g of Li into NSTX. The LITERs deposited Li on the lower divertor target for 10 min, at combined rates of 10–70 mg/min. Prior to each discharge, the LITERs were withdrawn behind shutters. The shutters remained close during a subsequent period of HeGDC. The shutters were then reopened and the deposition cycle repeated. The effects of Li edge conditions on standard discharge scenarios include: reduced plasma density in the early phase of the discharge, suppression of ELMs, improved energy confinement, reduced flux consumption and increased pulse length (for standard, high-triangularity discharges), reduced HeGDC time between discharges to maintain the H-mode, increased pedestal electron and ion temperature, and reduced SOL density and edge neutral density. Discharges after Li also benefited from $n = 1$ to 3 mode control by the external non-axisymmetric coils to reduce deleterious MHD activity.

Additional work is needed to determine the origin of the continued secular electron density rise and the respective contributions of recycling, increasing impurity confinement, and core impurity radiation with discharge duration, the nature and duration of the Li coatings, and the reduction in ELM occurrence. In conclusion, while additional work is required to resolve these issues, NSTX high-power divertor plasma experiments have shown that high-power diverted configurations benefit significantly from solid Li coatings applied to plasma facing components. These results are being applied to work in progress [16] on design and the forthcoming installation of the NSTX liquid Li divertor.

Acknowledgments

References

[1] M. Ono, S.M. Kaye, Y.-K.M. Peng, et al., Nucl. Fus. 40 (2000) 557.
[2] M.G. Bell et al., Nucl. Fus. 46 (2006) S565. and references therein.
[3] H.W. Kugel, M.G. Bell, R. Bell, et al., J. Nucl. Mater. 363–365 (2007) 791.
[4] H.W. Kugel, M.G. Bell, J.-W. Ahn, et al., Phys. Plasmas 15 (2008) 056118.
[5] V.A. Soukhanovskii et al., J. Nucl. Mater. 390-391 (2009) 516.
[6] D.K. Mansfield, D.W. Johnson, B. Grek, et al., Nucl. Fus. 41 (2001) 1823.
[7] R. Majeski, S. Jardin, R. Kaita, et al., Nucl. Fus. 45 (2005) 519.
[8] H.W. Kugel, R. Maingi, M. Bell, et al., J. Nucl. Mater. 337–339 (2005) 495.
[9] C.H. Skinner et al., J. Nucl. Mater. 390–391 (2009) 1005.
[10] S. Paul et al., J. Nucl. Mater. 390–391 (2009) 211.
[11] M.J. Baldwin et al., Nucl. Fus. 42 (2002) 1318.
[12] Y. Hirooka et al., J. Nucl. Mater. 363–365 (2007) 775.
[13] J.N. Brooks, J.P. Allain, T.D. Rognlien, R. Maingi, et al., J. Nucl. Mater. 337–339 (2005) 1053.
[14] W.R. Wampler et al., J. Nucl. Mater. 390–391 (2009) 1009.
[15] D.K. Mansfield, H.W. Kugel, R. Maingi, M.G. Bell, et al., Paper O-28 in this Conference.
[16] D. Stotler et al., Paper P3-01 in this Conference.